



Delft University of Technology

## Half a century of dynamic instability following the ocean-driven break-up of Wordie Ice Shelf

Dømggaard, Mads; Millan, Romain; Andersen, Jonas K.; Scheuchl, Bernd; Rignot, Eric; Izeboud, Maaïke; Bernat, Maud; Bjørk, Anders A.

### DOI

[10.1038/s41467-025-59293-1](https://doi.org/10.1038/s41467-025-59293-1)

### Publication date

2025

### Document Version

Final published version

### Published in

Nature Communications

### Citation (APA)

Dømggaard, M., Millan, R., Andersen, J. K., Scheuchl, B., Rignot, E., Izeboud, M., Bernat, M., & Bjørk, A. A. (2025). Half a century of dynamic instability following the ocean-driven break-up of Wordie Ice Shelf. *Nature Communications*, 16(1), Article 4016. <https://doi.org/10.1038/s41467-025-59293-1>

### Important note

To cite this publication, please use the final published version (if applicable).  
Please check the document version above.

### Copyright

Other than for strictly personal use, it is not permitted to download, forward or distribute the text or part of it, without the consent of the author(s) and/or copyright holder(s), unless the work is under an open content license such as Creative Commons.

### Takedown policy

Please contact us and provide details if you believe this document breaches copyrights.  
We will remove access to the work immediately and investigate your claim.

# Half a century of dynamic instability following the ocean-driven break-up of Wordie Ice Shelf

Received: 21 July 2024

Accepted: 11 April 2025

Published online: 29 April 2025



Mads Dømggaard <sup>1</sup>✉, Romain Millan <sup>2</sup>, Jonas K. Andersen<sup>1</sup>, Bernd Scheuchl <sup>3</sup>,  
Eric Rignot <sup>2,3,4,5</sup>, Maaïke Izeboud<sup>6</sup>, Maud Bernat<sup>7</sup> & Anders A. Bjørk <sup>1</sup>

Ice shelves restrain grounded ice discharge into the ocean, and their break-up contributes significantly to Antarctica's sea level rise. Using aerial imagery from the 1960s and modern satellite data, we construct a long-term record of Wordie Ice Shelf's disintegration and its effects on tributary glaciers. Early changes in pinning points and ocean warming in Marguerite Bay since the 1960s strongly suggest increasing basal melt as the primary driver of the ice shelf disintegration. Some glaciers responded immediately to the ice shelf break-up, with surface velocities tripling, thinning up to 160 m, and grounding line retreat of 7.5 km, while others reacted decades later due to buttressing from remnant parts of the ice shelf. Our findings emphasize the importance of long-term observations to understand ice shelf disintegration and its impacts, offering crucial insights for assessments of future ice loss from the Antarctic Ice Sheet.

Ice shelves, covering nearly two-thirds of Antarctica's coastline, are essential to the stability of the Antarctic Ice Sheet. Acting as buttressing forces, they regulate the amount of ice discharged into the ocean by glaciers flowing from the interior of the ice sheet<sup>1,2</sup>. The potential weakening and break-up of these ice shelves can have significant consequences for the grounded tributary glaciers, including rapid thinning<sup>3</sup>, velocity acceleration<sup>4</sup>, and grounding line retreat<sup>5</sup>, as observed during the collapse of Larsen B Ice Shelves in the Antarctic Peninsula, where the discharge of certain outlet glaciers more than tripled from 1996 to 2003<sup>6</sup>.

Ice shelf retreat styles vary widely, from rapid collapses to a protracted retreat<sup>7</sup>, and are driven by a wide range of factors<sup>8</sup>. These include atmospheric warming<sup>7,9</sup>, meltwater ponding and hydrofracturing<sup>10</sup>, brine infiltration<sup>11</sup>, increased basal melting from intrusion of warm circumpolar deep waters<sup>12,13</sup>, ice mélange removal<sup>14</sup>, and sea ice loss accompanied by ocean swell<sup>15</sup>. Moreover, ice shelf changes have been linked to damage and structural

weakening that precondition ice shelves for disintegration<sup>16–18</sup>, including the shifting role of pinning points, which can transition from stabilizing to destabilizing features during this process<sup>19–21</sup>. This emphasizes the complexity of ice shelf dynamics and stresses the critical need for long-term observations, as the initiation of ice shelf break-up may occur decades before their eventual disintegration<sup>21</sup>. Despite the limited availability of such observations, they are essential for improving our understanding of ice shelf behavior and establishing accurate baseline data for future modeling efforts<sup>21,22</sup>. Additionally, there is a notable lack of observations on the long-term impacts of ice shelf disintegration on tributary glaciers, which contributes to large uncertainties in projecting ice sheet contributions to future sea-level rise<sup>22,23</sup>. This is largely due to the fact that there are few observations of ice shelves that have disintegrated, as many of these events occurred prior to the availability of extensive satellite observations (e.g., Larsen A in 1995, Larsen B in 2002, Wordie in ~1980–1990s, Ostenfeld in 2004 in Greenland).

<sup>1</sup>Department of Geoscience and Natural Resource Management, University of Copenhagen, Copenhagen K, Denmark. <sup>2</sup>Univ. Grenoble Alpes, IRD, CNRS, INRAE, Grenoble INP IGE, Grenoble, France. <sup>3</sup>Department of Earth System Science, University of California, Irvine, CA, USA. <sup>4</sup>Department of Civil and Environmental Engineering, University of California Irvine, Irvine, CA, USA. <sup>5</sup>Caltech's Jet Propulsion Laboratory, Pasadena, CA, USA. <sup>6</sup>Department of Geoscience and Remote Sensing, Delft University of Technology, Delft, The Netherlands. <sup>7</sup>Université de Toulouse, LEGOS (CNES/CNRS/IRD/UT3), Toulouse, France. ✉e-mail: [mld@ign.ku.dk](mailto:mld@ign.ku.dk)

Since the early 20<sup>th</sup> century, the pursuit for polar exploration and mapping led to the acquisition of a large quantity of historical aerial images of Antarctica<sup>24–27</sup>. These archives present enormous potential for reconstructing the long-term evolution of Antarctic glaciers and ice shelves<sup>3,28</sup>, but remain underutilized<sup>29</sup>. In this study, we utilize more than 450 historical aerial images of the Wordie Ice Shelf, captured in November and December 1966 and January 1969, in combination with various satellite and climate datasets to conduct a comprehensive

analysis of its break-up along with the implications for the tributary glaciers.

The Wordie Ice Shelf is located in the Antarctic Peninsula, in Marguerite Bay (Fig. 1). Originally, multiple glaciers (Harriot, Fleming, Prospect, Carlson, and three unnamed glaciers, here called Foster Ice Piedmont (FIP) 1 and 2, and Unnamed) were flowing into the bay, forming a single unified ice shelf (Fig. 1), with Fleming being the largest and fastest among them. Around 1986 the ice shelf split into two parts<sup>19</sup>

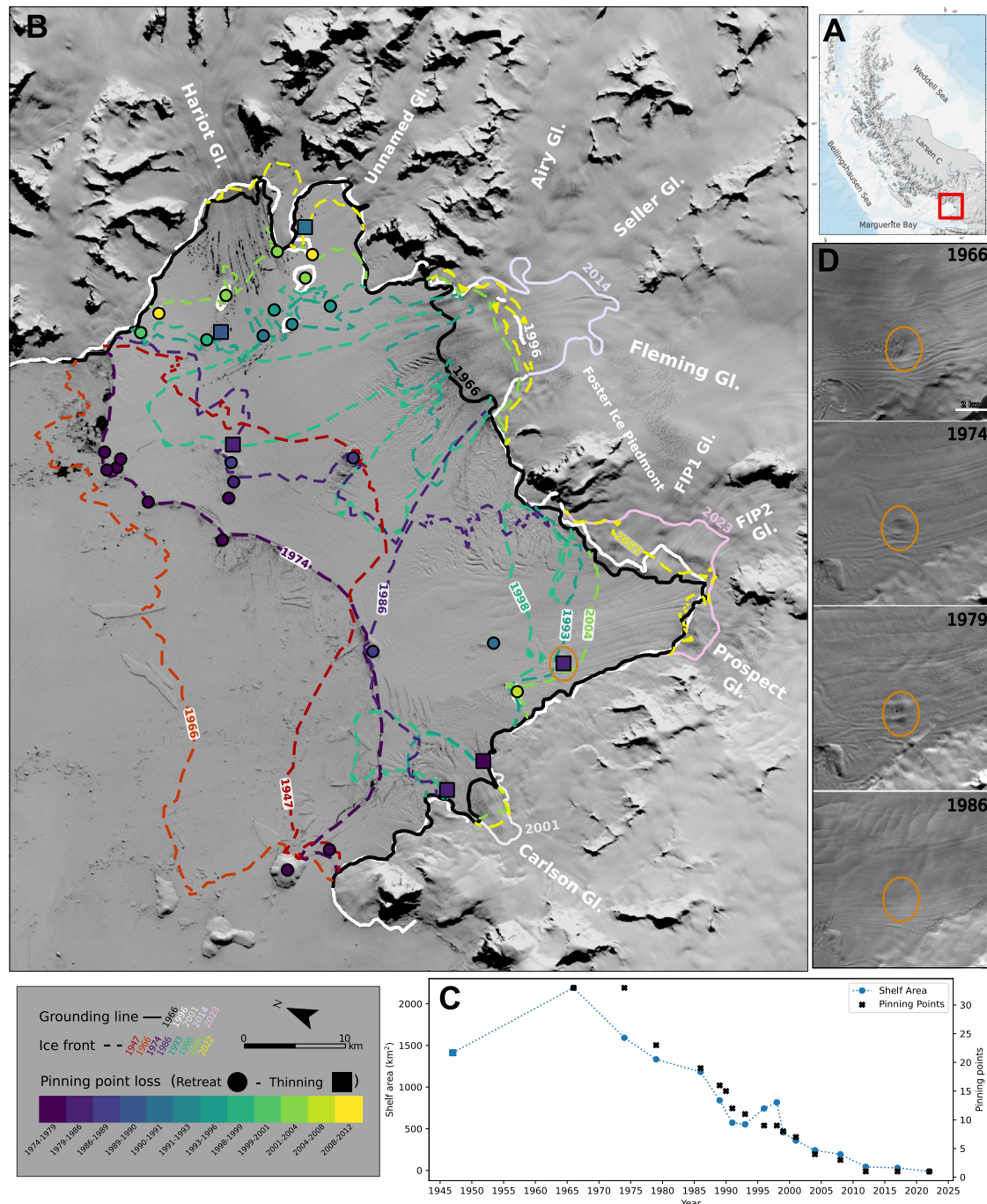


**Fig. 1 | Changes in ice shelf area and pinning points of the Wordie Ice Shelf.** **A** Location of Wordie Bay in the Antarctica Peninsula (made with Quantarctica<sup>70</sup>). **B** Evolution of ice shelf frontal position and pinning points 1947–2022, and 1966–2023 grounding line at Wordie Ice Shelf overlaid on a Landsat satellite image dated 06-01-1974. The 1966 grounding line is estimated from the historical DEM, while the 1996, 2001, and 2014 positions are sourced from existing datasets<sup>33,55,56</sup>. The 2023 grounding line positions at FIP1, FIP2, and Prospect glaciers

are estimated from optical satellite imagery (Methods). The pinning point color indicates the period of unpinning, while the symbol indicates the process of unpinning (circle = retreat, square = thinning). **C** Evolution in ice shelf area and number of pinning points 1947–2022. **D** Disappearance of a pinning point at the outlet of Prospect Glacier 1966–1986 due to thinning of the ice shelf. The location of the pinning point can be seen in (B).

and during the early 2000s it almost completely disintegrated, leaving behind a set of small individual ice shelves<sup>30</sup>. Doake and Vaughan<sup>19</sup> were the first to analyze fracture dynamics in this area, and attributed the initial disintegration to warming air temperatures and increased melt ponding<sup>19</sup>. However, their study was limited to only five images covering the ice shelf from 1974 to 1989. While numerous recent studies have investigated the region, their primary focus has been on the dynamic changes at Fleming Glacier during the more recent decades<sup>30–33</sup>, rather than on the processes underlying the ice shelf disintegration. Consequently, a detailed long-term investigation is essential to unravel both the climatic and glaciological factors contributing to the ice shelf disintegration, as well as the impacts on the tributary glaciers feeding into Wordie. Such information is crucial for determining the timing and time scales over which these ice shelf and glacier processes occur, offering critical insights into the mechanisms underlying ice shelf disintegration and enhancing our ability to project potential future changes in Antarctica.

## Results

After reaching its maximum observed extent of approx. 2200 km<sup>2</sup> in 1966, the Wordie Ice Shelf entered a period of nearly constant retreat and loss of pinning points (Fig. 1), which triggered substantial changes of the tributary glaciers. In the following section, we first describe the observed changes of the Wordie Ice Shelf, including variations in ice shelf size and elevation, pinning points, structural damages, and melt ponds. Subsequently, we examine the ice dynamic response of the tributary glaciers, focusing on changes in grounding line positions, ice flow velocities, and thinning rates.

### Ice shelf retreat and structural changes

In 1966 and 1974, ice shelf damage was limited, consisting mainly of transverse rifts found near the large pinning points, at the intersection between Fleming Glacier and FIP1-2 and Prospect Glacier, at the outflow of Carlson Glacier, and close to the 1966 Fleming Glacier grounding line (Fig. 1B, Supplementary Figs. S1, S2). From the historical 1966 DEM we estimate the median freeboard elevation of the ice shelf in front of Fleming, Harriot, and Unnamed Glacier to be 33 m ± 11 m (Supplementary Fig. S3) relative to sea level, which translates to an ice shelf thickness of 307 m ± 105 m (Methods). By 1979, the extent of ice shelf damage had increased, marked by larger and wider rifts and crevasses, and the emergence of longitudinal rifts, many originating upstream of the largest pinning points (Supplementary Fig. S2). This eventually led to the unpinning of many of these pinning points due to calving (Fig. 1B). Moreover, we observe unpinning occurring far from the ice shelf margin, driven by a thinning of the ice shelf (Fig. 1B.) Figure 1D illustrates the evolution of a pinning point at the outlet of Prospect Glacier, showing its gradual change between 1966 and 1979, culminating in its complete disappearance by the next available image in 1986. Unfortunately, precise thinning rates cannot be quantified from the available historical data.

In 1979, Carlson Glacier started disconnecting from the ice shelf, and by 1986 it had lost both its pinning points at the ice front where the glacier flow becomes unconfined (Fig. 1B). By 1986, Wordie Ice Shelf split into two separate parts: i) a Western part, consisting mainly of Prospect Glacier, FIP1 and FIP2, and ii) an Eastern part consisting of Fleming Glacier, Harriot, and Unnamed Glacier (Fig. 1B). By 1990, the main branch of the Fleming ice shelf was completely disconnected from Harriot and Unnamed, removing all lateral drag, and subsequently retreated ~19 km (Supplementary Fig. S4). Simultaneously, the connected ice shelf of Prospect Glacier, FIP1, and FIP2 retreated to a confined area (Supplementary Figs. S2, S4). The increase in ice shelf size during the 1990s is mostly related to a re-advance of the main branch of Fleming and (to a lesser extent) Carlson glaciers. After the re-advance, the ice shelf area decreased markedly, and at Harriot and Unnamed glaciers pinning points were lost at the ice shelf front both

due to retreat and thinning (Fig. 1B, C). Between 1996 and 1998 large crevasses propagated far inland at Flemming Glacier, preceding its near-complete disappearance around 2000 (Supplementary Figs. S2, S5). Similarly, Carlson Ice Shelf had nearly vanished by 2002, while Harriot and Unnamed Ice Shelves disappeared by 2009 and 2023, respectively (Supplementary Figs. S2, S4). Additionally, the combined ice shelf of Prospect Glacier, FIP1, and FIP2 disintegrated between 2012 and 2014 (Supplementary Fig. S4).

Surface melt ponds are predominantly observed on the eastern sector of the Wordie Ice Shelf near Harriot and its neighboring glaciers (Fig. 1), with initial observations of meltwater ponding dating as far back as December 1966 (Supplementary Fig. S6). Moreover, thanks to the high resolution of the orthomosaics, small ponds (<0.025 km<sup>2</sup>) were detected in front of Fleming Glacier in 1969 (Supplementary Fig. S7). On the ice shelf in front of Harriot Glacier, large melt ponds persistently appeared until 1991 (Supplementary Fig. S6). By 2001, the melt ponds had mostly disappeared, with only small ponds remaining, primarily at the smaller glaciers adjacent to Harriot. As cloud-free optical imagery was unavailable from 1992 to 2001, the melt ponds could have extended into the late 90s. Moreover, there are notable annual variations in the area and location of melt ponds (Supplementary Fig. S6), with the largest single melt pond (~6 km<sup>2</sup>) observed on January 12, 1969. These variations may partly reflect seasonal differences in acquisition times, as images captured close in time show different pond distributions. Due to sparse image availability, we cannot rule out that melt ponds have been present at other parts of the ice shelf during the early stages of the disintegration. However, we consider this unlikely, as no melt ponds were observed in any other areas of the ice shelf during years when image coverage was more consistent.

### Acceleration, grounding line retreat and thinning of tributary glaciers

Figures 2 and 3 presents the evolution of ice velocities, grounding line positions, and ice elevation for the Wordie Bay glaciers between 1966 and 2023, illustrating a variable dynamical response between the glaciers during the disintegration of Wordie Ice Shelf.

At Carlson Glacier, velocities nearly doubled from ~500 m/yr in 1966 to ~950 m/yr in 1986 at the 1966 grounding line position, followed by a further 40% increase to ~1350 m/yr in 1989 (Fig. 2). Similarly, Fleming Glacier experienced a 50% velocity increase from ~1100 m/yr in 1966 to ~1700 m/yr in 1986 at the 1966 grounding line, with a subsequent rapid acceleration between 1989 and 1991, rising from ~1900 m/yr to ~3200 m/yr (Fig. 2). Since the early 1990s, velocities were relatively stable, except for a ~300 m/yr decrease at Carlson Glacier between 2000 and 2007 and an acceleration of both glaciers from 2007 to 2013. Moreover, during the initial observation period from 1966 to 1996/2001, the grounding line of Fleming Glacier retreated by 7.5 km (Fig. 2), while Carlson Glacier experienced a retreat of 6.6 km. By 2014, the grounding line at Fleming Glacier had retreated an additional ~5.5 km (Fig. 2). The early changes in grounding line position and velocity acceleration were accompanied by  $160 \pm 14.6$  m of thinning at the grounded section of Fleming Glacier between 1966 and 2007 (Method). This corresponds to a thinning rate of  $4.0 \pm 0.4$  m/yr (Fig. 3A), exceeding the 2007–2022 rate of  $3.2 \pm 0.7$  m/yr (Fig. 3B).

In contrast to the early dynamic response of Carlson and Fleming glaciers, FIP1, FIP2, Prospect, Harriot, and Unnamed glaciers show minimal changes in grounding line and ice velocity during the first three decades, with the most substantial changes occurring over the past two decades (Fig. 2). On the eastern part of the ice shelf, grounding line positions remained stable from 1966 to 1996, with no detectable retreat at Unnamed Glacier and only 1.1 km at Harriot Glacier. No grounding line estimates are available after 1996 for these glaciers (Methods). At Harriot Glacier the most notable velocity acceleration occurred between 1994 and 2000, with an increase of around



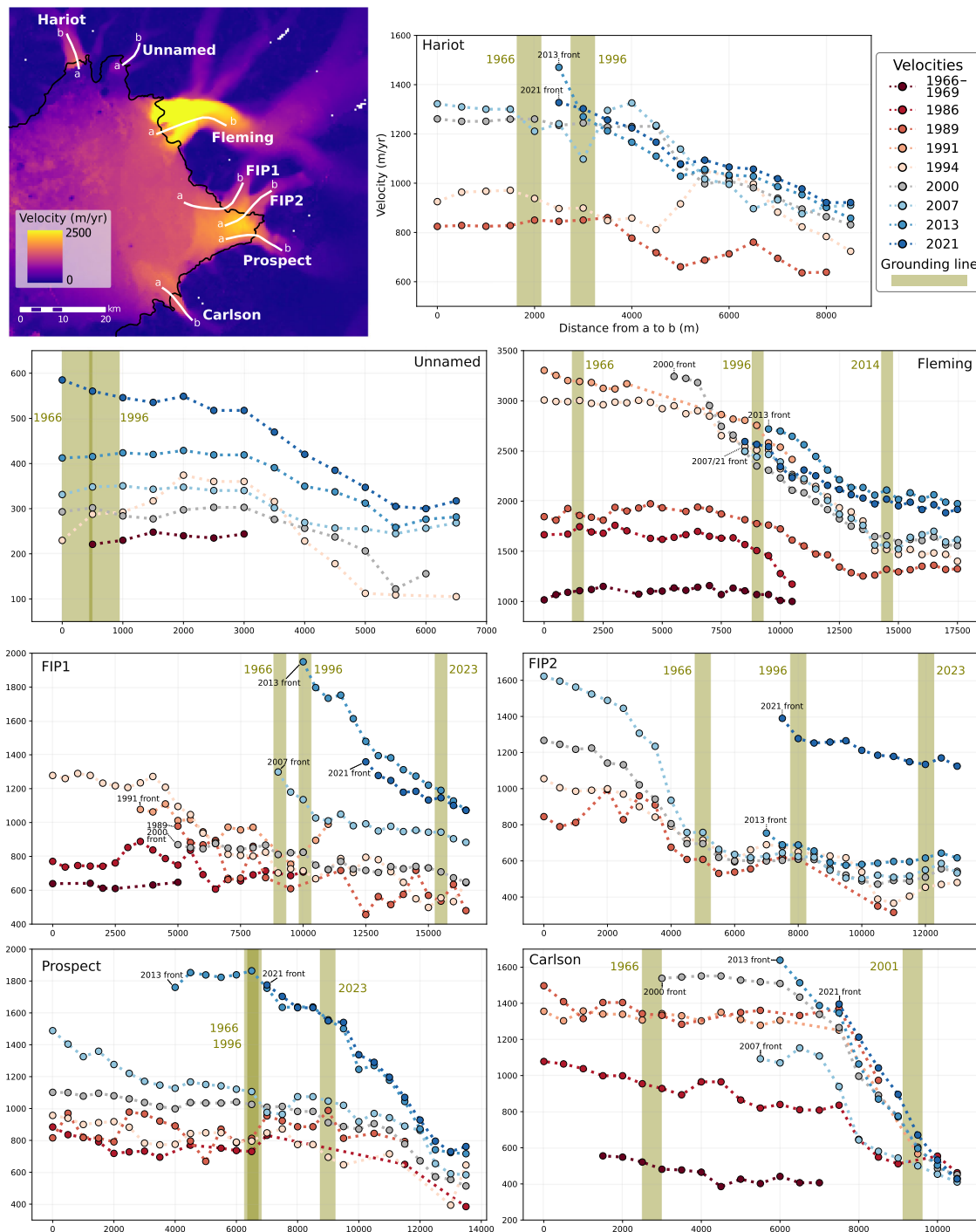


**Fig. 2 | Surface velocity and grounding line change of Wordie Ice Shelf tributary glaciers.** Velocities and grounding line positions are measured along a given transect from a to b, as seen on the overview map showing the 2021 mean annual velocity. Historical velocities for Carlson Glacier are derived from orthomosaic pairs captured in 1966, while those for Fleming, FIP1, and Unnamed glaciers utilize

pairs from both 1966 and 1969, with an uncertainty of 60 m/yr. Velocities spanning 1986–2021 were calculated using feature and speckle tracking of satellite observations with a mean uncertainty of 38 m/yr (Methods). For each year, we exclude all measurements seaward of the frontal position to avoid comparing velocities over sea ice or mélange. Note that the x and y-axes differ among glaciers.

40% (–900 m/yr to –1250 m/yr) at the grounding line. At Unnamed Glacier, we observe velocity fluctuations ranging from –220 to 330 m/yr from 1966 to 2007, with the lowest velocities recorded in 1966. The largest flow acceleration occurred between 2013 and 2021, with an increase from –400 m/yr to –550 m/yr (Fig. 2). At Hariot Glacier, thinning rates remained similar from 1966–2007 to 2007–2022, whereas at Unnamed Glacier, rates more than doubled from  $0.7 \pm 0.4$  m/yr in 1966–2006 to  $1.5 \pm 0.7$  m/yr in 2007–2022. On the western part of the

ice shelf, the grounding line of Prospect Glacier was stable from 1966 to 1996 but retreated 2.5 km from 1996 to 2023. Similarly, FIP1 exhibited a retreat of less than 1 km between 1966 and 1996, followed by a more substantial retreat of 5 km from 1996 to 2023. At FIP2 there was a total retreat of 7 km, with 4 km occurring after 1996. Historical velocities could only be extracted from the floating part of the ice shelf at FIP1, where the velocity doubled between its 1966 minimum and the 1994 maximum (Fig. 2). In contrast, near the 1966 and 1996 grounding

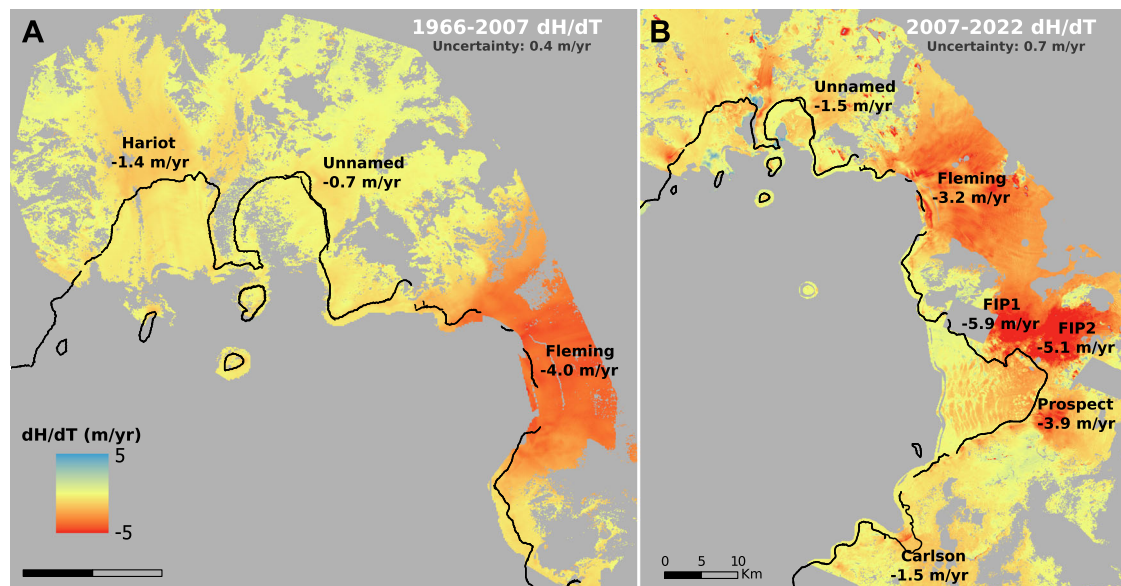


**Fig. 3 | Elevation change rates (dH/dT) of Wordie Ice Shelf tributary glaciers.** **A** dH/dT from 1966 to 2007 for Hariot, Unnamed and Fleming Glacier calculated from the 1966 Historical DEM and the 2007 SPOT DEM, with an estimated uncertainty of 0.4 m/yr (Methods). Due to incomplete coverage of the 1966 historical

DEM (Methods) elevation change rates cannot be calculated for the remaining glaciers. **B** dH/dT from 2007 to 2022 for all glaciers, calculated from the 2007 SPOT DEM and 2022 REMA Strip Mosaic, with an estimated uncertainty of 0.7 m/yr.

line, there were limited velocity changes between 1986 and 2000, ranging from  $-600$  m/yr to  $850$  m/yr. Between 2000 and 2013, the velocity more than doubled, increasing from  $-850$  m/yr to  $-1900$  m/yr, with a slight subsequent decrease in 2021 (Fig. 2). At FIP2, velocities at the 1996 grounding line remained relatively stable from 1989 to 2013, after which they accelerated rapidly from  $-700$  m/yr in 2013 to  $-1300$  m/yr in 2021. The velocity at Prospect Glacier accelerated gradually from 1986 to 2007 at the 1966/1996 grounding line, after which we observed a large acceleration from  $-1100$  m/yr in 2007 to  $-1850$  m/yr in 2013 (Fig. 2). Unfortunately, no historical elevation data is available for Prospect and FIP1-2 glaciers. However, between 2007 and 2022, all experienced significant thinning, with rates ranging from  $3.9 \pm 0.7$  m/yr to  $5.9 \pm 0.7$  m/yr, the highest at FIP1 (Fig. 3).

## Discussion

On the Antarctic Peninsula, the break-up of ice shelves, including Wordie, have been linked to rising air temperatures leading to melt ponding and hydrofracturing<sup>19,34,35</sup>. At Rothera Station 150 km from Wordie Bay (Supplementary Fig. S9), mean austral summer temperatures increased by approximately  $1^\circ\text{C}$  from the earliest observations in mid-1970s to the peak in the early 1990s, followed by a slight decrease and 30 years of relative stability (Fig. 4). The consistent presence of meltwater ponding on Wordie since the 1960s (Fig. 4 and Supplementary Fig. S6) indicates long-term high summer temperatures and ablation in the region and predates the temperature records from Rothera by a decade. Melt ponds are predominantly observed in the part of the ice shelf that disintegrated last, with no evidence of such features in the outer sections that calved during the initial stages of disintegration. This contrasts with the disintegration of Larsen B, where extensive meltwater lakes developed across the entire ice shelf in the two decades preceding its rapid collapse in 2002<sup>36</sup>. Collectively, this evidence suggests that the Wordie Ice Shelf was likely accustomed to excess surface meltwater, with the possibility of a firn aquifer in the region, and that melt ponding and hydrofracturing may have played a limited role in its early disintegration. However, due to sparse image availability during the early decades we cannot completely rule out this mechanism. During later stages, meltwater may have deepened

shallow crevasses<sup>10</sup>, such as those at Fleming, through hydrofracturing, further destabilizing the ice shelf. ERA5 summer temperatures from Wordie Bay, show an increase of more than  $1^\circ\text{C}$  from the record low in 1948 to the early 1960s (Fig. 4), during a time when the shelf area grew substantially (Fig. 1) This is followed by a  $-0.5^\circ\text{C}$  dip in the late 1960s and a subsequent  $-0.5^\circ\text{C}$  increase towards the 1980s, when the first important ice shelf split occurred (Fig. 4). However, the accuracy of atmospheric reanalysis data for Antarctica before the 1980s is largely constrained by the scarcity of historical observations<sup>37</sup>.

Changes in pinning points are commonly used as indicators of ice shelf thickness variability<sup>38</sup>, and the loss of pinning points located far from the Wordie Ice Shelf front provides clear evidence of sustained thinning since the 1970s (Fig. 1D). Ice shelf thinning is primarily driven by the intrusion of warm Circumpolar Deep Water (CDW) onto the continental shelf, inducing basal melting of the ice shelves<sup>13</sup>. Recent studies have found that warm CDW from the Antarctic Circumpolar Current (ACC) periodically flows onto the shelf of Marguerite Bay<sup>31</sup>, with high basal melt rates of  $24 \pm 10$  m/yr reported at the remainder of the Wordie Ice Shelf from 2003 to 2008<sup>39</sup>. Measurements of mid-ocean temperatures in the Wordie Bay region increased by more than  $0.3^\circ\text{C}$  between 1960 and 1990 (Fig. 4), coinciding with the onset of ice shelf retreat and period when the first major disintegration event occurred. The ongoing thinning, driven by increased basal melting that changes linearly with temperature<sup>40</sup>, progressively weakened the Wordie Ice Shelf, leading to the development of larger and wider rifts and crevasses, particularly near pinning points and along the shear margin. While the pinning points provided critical buttressing during the early retreat phase, over time, they became sources of fractures and rifts that expanded upstream, ultimately contributing to the ice shelf's destabilization<sup>19</sup>. The re-growth of the ice shelf during the 1990s (Fig. 1) coincides with a sustained period of dense ice mélange (Supplementary Fig. S5), which remained largely intact, likely due to stable ocean temperatures (Fig. 4), high sea ice concentration (Supplementary Fig. S8), the presence of high bathymetric sills, and its base being mostly above the CDW layer in Wordie Bay<sup>41</sup>. This likely stabilized the retreat of the ice shelf front and favored a re-advance in this period. Ice mélange has been associated with ice shelf stability, and its sudden

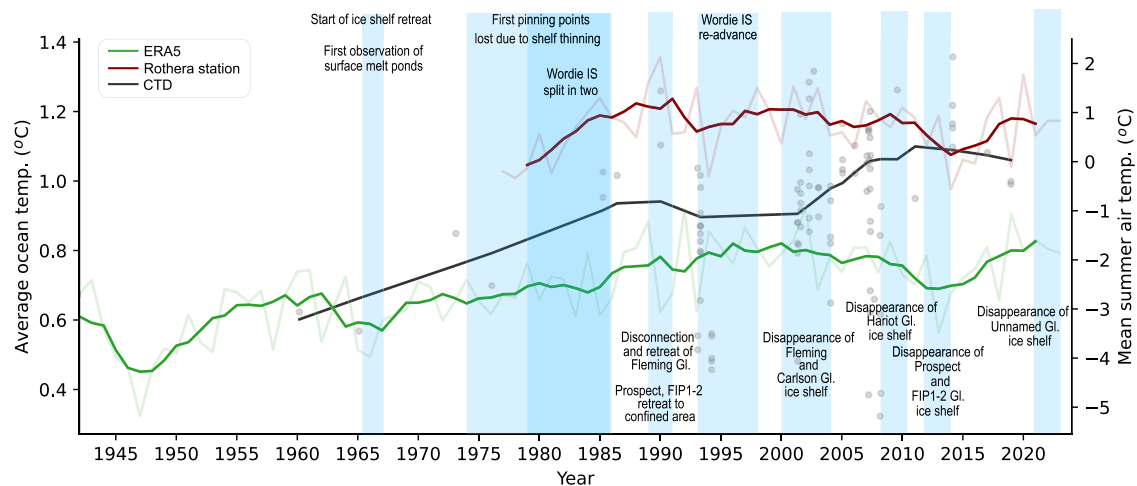


**Fig. 4 | Overview of key changes at the Wordie Ice Shelf in relation to the evolution of average mid-ocean and summer air temperatures.** The mean summer air temperature (December, January, and February) from Rothera Station (1976–2023) (red line) and ERA5 2 m temperature estimates for the Wordie region

(1941–2023) (green line) plotted as 5-year running averages. Average mid-ocean temperatures (150–500 m depth) were calculated from CTD measurements in Marguerite Bay (1960–2019) (black line), with individual measurements shown as circles (Methods).

removal has been linked to ice shelf retreat<sup>14,18</sup>. Indeed in 1999, more than half of the ice mélange in Wordie Bay dispersed (Supplementary Fig. S5) and completely disappeared by the 2000s, marking the onset of a new retreat phase that culminated in the ice shelf's disappearance (Fig. 1). However, the minor changes in surface speeds following the mélange's dispersal (Fig. 2) suggest it played a limited role in buttressing glacier ice discharge<sup>42</sup>, though it appears to have stabilized the front between 1990 and 1998. These observations highlight the complex interplay of processes influencing Wordie Ice Shelf while underscoring the oceanic influences on the ice shelf's existence. Together with the findings detailed earlier, our results strongly suggest that warming ocean temperatures have been the primary factor contributing to the disintegration of the Wordie Ice Shelf, contrasting with previous studies that emphasized atmospheric warming and hydrofracturing as primary contributors<sup>19</sup>.

The tributary glaciers feeding into the Wordie Ice Shelf display highly variable responses to its disintegration. Carlson and Fleming glaciers showed an early response to the ice shelf disintegration, with multiple phases of large velocity accelerations between 1966 and 1991, resulting in a 170% and 190% speed-up, respectively (Fig. 2). These results align with studies of Fleming Glacier finding a 50% acceleration between 1974 and 1996–50 km upstream from the 1996 grounding line<sup>32</sup>, with no notable changes between 1996 and 2008<sup>30</sup> (Fig. 2). Our historical reconstructions also reveal that this early speed-up was followed by a 7.5 km grounding line retreat and a 160 m dynamic thinning, exceeding the changes observed in the following two decades (Figs. 2 and 3). Similarly, we find it likely that most of the 6.6 km grounding line retreat observed at Carlson Glacier from 1966 to 2001 occurred during the rapid acceleration from 1966 to 1989. These sudden changes of both Carlson and Fleming Glacier may be attributed to the loss of major pinning points and a disconnection from the greater ice shelf area, occurring between 1979 and 1990. This disconnection allowed for less restricted flow, as the main ice tongue became unconfined, losing lateral and frontal contact with neighboring ice shelf parts, hence largely reducing the buttressing potential<sup>43</sup>.

The dynamic responses of the remaining glaciers feeding into Wordie Ice Shelf (FIP1-2, Prospect, Harriot, and Unnamed Glacier) were slower, less pronounced, and occurred much later in time (Figs. 2 and 3). Following the greater shelf disintegration in the late 1980s to early 1990s, the connected ice shelf area of FIP1, FIP2, and Prospect Glacier retreated to a confined position, maintaining lateral resistance and providing buttressing for these glaciers. As a result, the largest

velocity acceleration and grounding line retreats occurred in the last two decades (Fig. 2), when this ice shelf completely disintegrated. This disintegration also triggered extensive dynamic thinning, with FIP1 and FIP2 glaciers experiencing the highest elevation change rates of any tributary glaciers during any period, from 2007 to 2021 (Fig. 3). Similarly, Harriot and Unnamed glaciers showed no immediate response to the disintegration of the greater ice shelf as they remained confined, maintaining lateral contacts with the fjord walls. Instead, the most significant acceleration at the grounding line (Fig. 3) occurred between 1994–2000 at Harriot and 2013–2021 at Unnamed Glacier, during times of frontal retreat and loss of important pinning points (Fig. 1, Supplementary Fig. S4C). Thinning rates at Unnamed Glacier more than doubled from 1966–2007 to 2007–2022, while they remained largely unchanged at Harriot Glacier, due to the disintegration and speed-up occurring within the time span of the first two DEMs.

Other studies have focused on more recent changes at Fleming Glacier, identifying a large increase in flow speed and elevation draw-down around 2008<sup>31,33</sup>. This has been attributed to enhanced melting at the ice-ocean interface, driven by strong La Niña conditions and a positive Southern Annular Mode (SAM), which altered wind patterns, as well as to the 1996–2014 grounding line and related unpinning<sup>33</sup>. However, on a longer timescale, this recent 20% speed-up observed at the Fleming Glacier 1996 grounding line<sup>31,33</sup> appears relatively modest compared with the 50% and 60% accelerations from 1966 to 1986 and 1989 to 1991, respectively (Fig. 3). Overall, the observed flow acceleration, thinning and grounding line retreat of the tributary glaciers feeding into Wordie Bay since the 1960s reveal a substantial increase in ice discharge. Given that the trend in estimated surface mass balance (SMB) has remained constant since 1979 (Supplementary Fig. S9), the glaciers have been collectively experiencing a decrease in net mass balance for more than 50 years. As our observations predate early estimates of Antarctic mass loss<sup>44</sup>, there is a possibility that ice loss from the Antarctic Peninsula has been underestimated. This is further supported by evidence of marine-terminating glaciers retreating in some areas since the 1940s and more extensively across the Western Peninsula since the 1960s<sup>45</sup>, with a link to ocean-induced melting<sup>46</sup>. However, to fully interpret and understand the effects of warming ocean temperatures, accurate bathymetry data is crucial<sup>47</sup>, yet it remains missing for many key region of Antarctica, including Wordie Bay.

Our results reveal that Wordie Ice Shelf has been continuously disintegrating since the 1960s, primarily driven by basal melting from



warming ocean temperatures, in contrast to previous studies that attributed the break-up to atmospheric warming<sup>19</sup>. The break-up led to extensive thinning, velocity acceleration, and grounding line retreat of the tributary glaciers, with the most pronounced changes at Fleming Glacier. Notably, the tributary glaciers exhibited varied response times, with some reacting immediately while others exhibited a delayed response several decades later. A similar pattern was observed after the collapse of Larsen B<sup>6</sup>, albeit over a much shorter timeframe, and highlight several crucial aspects of the interplay between ice shelf and ice sheet dynamics. First, they emphasize the critical role of ice shelves in stabilizing tributary glaciers. Secondly, they demonstrate that current ice loss may be a delayed consequence of ice shelf disintegration events that occurred decades ago, underscoring the importance of combined long-term observations on ice shelf retreat and glacier responses. One of the major challenges in predicting future ice loss is determining how calving may undermine ice shelf buttressing and trigger dynamic glacier responses<sup>1</sup>. Our results highlight the need for a more nuanced understanding and accurate parameterization of the complex interactions between ice shelves and tributary glaciers in ice sheet models, to improve future sea level projections. Additionally, our findings underscore the vulnerability of ice shelves to gradual changes in oceanic forcing and highlight the need for extended time series to better understand the processes driving ice shelf disintegration, thereby enhancing our ability to detect early warning indicators in other parts of Antarctica.

## Methods

### American Aerial photographs

We utilize 468 black and white aerial photographs of the Wordie Ice Shelf collected mainly by the US NAVY from 1966 to 1969 (Table 1). The images were captured using a trimetrogon camera setup, wherein left-oblique, on-nadir (vertical), and right-oblique images are captured simultaneously<sup>27</sup>. Coverage of the Wordie Bay region varies across years, with the November 28, 1966 images providing nearly complete coverage.

We process the images using a standard structure from motion workflow<sup>48</sup> in Agisoft Metashape v. 2.0.2, with photographs from different years processed separately. Over the eastern part of the ice shelf, including Fleming, Unnamed, and Hariot glaciers, sufficient visible bedrock enabled the generation of a DEM with accurate absolute elevations from the November 28, 1966 images (Supplementary Fig. S3). For the remaining study area and images from other dates, limited visible bedrock allowed for the production of only relative DEMs and orthomosaics.

First, the images are scaled and aligned by detecting the image fiducials using the Detect Fiducial function. All fiducials are manually inspected and misplaced ones are corrected. Subsequently, the images are aligned by extracting up to 50,000 key points per image. In certain instances, additional tie points are manually placed to ensure precise image alignment. To produce the absolute DEM from November 28, 1966, 42 ground control points (GCPs) were manually placed in the aerial images. The GCPs are distinct stable bedrock features that can be identified in both the historical imagery and the 2 m resolution Reference Elevation Model of Antarctica (REMA) Mosaic<sup>49</sup>, which

serves as the reference model. For the relative DEMs and orthomosaics, this step is unnecessary, as georeferencing occurs later in the workflow. Next, we generate a dense point cloud at maximum image resolution, and obvious outliers are manually filtered. The dense point cloud is then gridded into a DEM and used to create a mesh, from which the orthomosaics are generated.

The relative orthomosaics and DEMs are georeferenced to 15 m resolution panchromatic Landsat 8 satellite imagery of the Wordie Bay region. The orthomosaics and DEMs are generated at similar pixel resolution, which allows us to transfer the GCPs from the orthogeorectification to the DEM. We georeference the orthomosaic using distinct surface features such as nunataks and islands and distribute the control points evenly across the image. To constrain the georeferencing over the ice shelf area, we use ice rises detectable in the 1974 and 1979 Landsat images. However, we acknowledge that these points may exhibit larger uncertainties compared to the control points over stable bedrock. The georeferencing is performed using an affine transformation, with the number of control points placed varying from 15 to 25 depending on the coverage of the orthomosaic. The georeferenced orthomosaics have a resolution of 4–6 m and a Root Mean Square (RMS) error from the placed control points ranging from 40.1 to 43.2 m. Among the three generated orthomosaics, the one from November 28, 1966 is based on the largest selection of images (Table 1) and provides the most extensive and complete coverage of the entire ice shelf area, along with the glaciers flowing into it (Supplementary Fig. S1). For the georeferencing of this orthomosaic a total of 25 control points were placed, achieving an RMS error of 41.8 m. Following the georeferencing of the orthomosaic, we transfer the GCPs to the corresponding DEM to ensure consistent georeferencing between the two products. Despite the relative elevations of the precisely georeferenced DEMs, they are still useful for accurately detecting changes in slope.

### DEM post-processing and glacier elevation change

First, the historical absolute DEM from November 28, 1966 is clipped to the minimum boundary area defined by the placed GCPs<sup>28</sup>. Next, the clipped DEM is co-registered<sup>50</sup> to the REMA reference DEM, and the uncertainty is estimated to 11.2 m based on the Normalized Median Absolute Deviation (NMAD) of the elevation differences over stable bedrock<sup>51</sup>.

To analyze elevation changes over time, we incorporate two additional DEMs: one from 2007 and another from 2022. The 2007 DEM, was generated from SPOT5-HRS stereopair images captured on February 21, 2007<sup>52</sup> using the Ames Stereo Pipeline software<sup>53</sup> with an initial co-registration to the Copernicus (GLO-30) DEM. After a filtering step, the SPOT DEM was vertically adjusted with synchronous ICESat altimetry data (closest campaign in time). An additional co-registration to the REMA reference DEM Mosaic was performed giving an estimated uncertainty of 9.3 m. The 2022 DEM is created by mosaicking multiple REMA strips acquired over a short time span from November 22, 2021 to April 6, 2022 to minimize errors due to variable ice cover. Each strip is individually co-registered before mosaicking, with the final DEM assigned a date of January 28, 2022 and an estimated uncertainty of 5.4 m. For each glacier we estimate changes by calculating the mean elevation differences within an area located behind the 2022 frontal position and the 1996 grounding line (Supplementary Fig. S10) during the two periods 1966–2007 and 2007–2022.

From the 1966 DEM we estimate the ice shelf freeboard elevation relative to sea level by calculating the median elevation of the ice shelf area defined by the 1966 grounding line position. From this freeboard elevation we determine the 1966 ice shelf thickness by setting the density of the shelf ice and seawater to 917 kg/m<sup>3</sup> and 1027 kg/m<sup>3</sup>, respectively.

**Table 1 | Overview of all utilized aerial images**

Flightline	Date	Number of Images
1834	November 28, 1966	150
1835	November 28, 1966	156
1843	December 27, 1966	6
1844	December 27, 1966	51
1845	December 27, 1966	36
2167	January 12, 1969	69



## Grounding line location

Historical grounding line positions from 1966 are determined using the break of slope method from Mougnot et al.<sup>54</sup>, with an uncertainty of 500 m. The grounding line mapping is performed using a slope and a hillshade raster (Supplementary Fig. S11), generated from the November 28, 1966 georeferenced historical DEM at 100 × 100 m resolution to even out local errors. In addition to the historical grounding lines, we incorporate MEaSUREs 1996 data derived from Differential Synthetic Aperture Radar (DInSAR) data<sup>55</sup>. However, as no DInSAR grounding line is available for Carlson Glacier, we utilize the data from Antarctic Surface Accumulation and Ice Discharge (ASAIID)<sup>56</sup> project derived from the break of slope using Landsat 7 imagery and ICESat altimetry data with a temporal coverage from 1999 to 2003<sup>57</sup>.

In an effort to retrieve recent grounding line locations, we used DInSAR measurements from the EU/ESA Sentinel-1 satellites and the conventional method of double-difference interferometry<sup>58</sup>. We processed 200 image pairs from 2016 to 2023 with a temporal baseline of 6 days (when available, otherwise 12 days). However, in all cases, interferometric coherence was consistently lost over the full region of interest, meaning that no useful vertical displacement measurements could be extracted. Applying the method of differential range offset tracking<sup>59</sup> to the Sentinel-1 measurements equally did not yield meaningful measurements. This limitation may be due to the difficulty of tracking the GL with DInSAR for a relatively small floating section (e.g. limited resolution and loss of coherence due to precipitation, surface melting, or fast ice flow and high deformation).

Modern grounding line estimates from 2014 are available for Fleming Glacier<sup>31,33</sup>, with notable disparities in the findings. Friedl et al.<sup>33</sup> suggest the grounding line to be situated 5–8 km further upstream than Walker and Gardner<sup>31</sup>. We have opted to adopt the Friedl et al.<sup>33</sup> estimate, as they calculate the hydrostatic equilibrium of the glaciers center, whereas Walker and Gardner<sup>31</sup> refer to the 1996 grounding line. Moreover, utilizing optical satellite imagery<sup>60</sup> we determine approximate 2023 grounding lines for FIP1, FIP2, and Prospect Glacier. This methodology is employed only when the surface shading in the optical satellite imagery provides a clear distinction between the grounded and floating sections of the glacier (Supplementary Fig. S12). As a result, we are unable to determine optical-derived grounding lines for Harriot, Unnamed, Carlson, and Fleming Glacier. By comparing the 1996 DInSAR grounding line to the break of slope from the surface shading in the 1990 optical images (Supplementary Fig. S12), we observe a close alignment with the largest variation of 1000 m observed at the FIP2. The average variation is ~300 m between the grounding line estimates.

The grounding zone marks the region where the glacier transitions from being completely grounded to floating. As a result the different mapping techniques map features within the grounding zone that act as proxies for the true grounding line<sup>60</sup>. Consequently, some of the changes observed in the grounding line may be attributed to variations in the mapping method, and to the tide magnitude at the time of measurement. However, due to the close alignment between 1996 DInSAR and the 1990 break of slope grounding line (Supplementary Fig. S12), we anticipate this factor to have minimal influence.

## Ice velocity

We compile a time series of surface ice velocities spanning over 50 years by integrating data from multiple satellites and aerial orthomosaics. Velocities from 1966 to 1969 are obtained from orthomosaics, which are precisely georeferenced prior to feature tracking using stable bedrock areas. For three glaciers (Unnamed, Fleming, and FIP1), we manually track the movement of distinct surface features on the glacier and ice shelf surface between 28-11-1966 and 12-01-1969. The uncertainties of the manual tracking are determined as

the combined uncertainty of the georeferencing error and the manual error attributed to feature positioning which is set to 1 pixel. This approach gives a combined uncertainty of 60 m/yr. For the Carlson glacier, the relatively short time between repeat acquisitions, approximately 1 month (28-11-1966 and 27-12-1966), enables us to employ automatic feature tracking. We first perform a sobel filter in the x and y direction to enhance surface features on images. Finally, we feed the resulting images to the feature tracking algorithm using image correlation windows of 64 × 64 pixels, search windows of 20 × 20 pixels with spacing of 10 pixels. From 1986 to 2021, we use time series of surface flow velocities originating from feature and speckle tracking using satellite observations from ESA's ERS-1&2, Sentinel-1a/b and Sentinel-2, RADARSAT-1&2, JAXA's ALOS/PALSAR, NASA's LANDSAT-1-8. The methodology follows the approaches described by Mougnot et al.<sup>61</sup>, Mougnot et al.<sup>62</sup>, and Millan et al.<sup>63</sup>, with velocities exhibiting a mean uncertainty of 38 m/yr, ranging from 29 to 55 m/yr. To account for missing years of interest, we augment the time series with data from the ITS\_LIVE annual mosaics<sup>64</sup>. Velocities are extracted along an approximate center flowline of each glacier. The flowlines are positioned as close to the center as possible, with slight adjustments made based on areas with the most complete historical velocity estimates. For each year, we exclude all measurements seaward of the frontal position to avoid comparing velocities over sea ice or melange.

## Ice shelf area and pinning points

Frontal positions of the Wordie Ice Shelf and its glaciers spanning 1966–2022 are mapped using the generated orthomosaics and the optical Landsat images (1974–1991 and 2001–2022), with a preference for images captured during the austral summer. The ice shelf area is determined with respect to the MEaSUREs 1996 grounding line. We also supplemented our analysis with data from ESA's ERS-1 and ERS-2 satellites in the period 1991–2004. Single Look Complex (SLC) images were processed into amplitude and geocoded using the 200 meter resolution DEM from the Radarsat Antarctic Mapping Project (RAMP). Given the lower resolution of ERS backscatter images and distortions due to the different satellite geometries, the frontal positions from 1992 to 2000 are more difficult to accurately delineate than for the Landsat data.

We map all ice shelf pinning points found in both the 1966 orthomosaic and 1974 Landsat images to exclude ephemeral features, as these may gain contact or unpin due to tidal processes and thus provide limited buttressing<sup>65</sup>. Subsequently, we map when the ice shelf unpins from the pinning point either due to thinning or due to retreat (Figs. 1 and 2). However, during the period from 1993 to 1999, the low resolution and high distortion levels of the ERS radar images prevent us from determining whether pinning points disappeared due to thinning.

## Climate, SMB, ocean, and sea ice concentration of Wordie region

We extract RACMO 2.3p2 mean annual surface mass balance (SMB), snowfall, and rainfall from 1979 to 2022<sup>66</sup> for the Wordie region (Supplementary Fig. S9). Additionally, we calculate the mean austral summer temperature (December, January, February) from 1941 to 2022 using 0.25° ERA5 data<sup>67</sup> and since 1976 using observational records from Rothera Station located approx. 150 km from Wordie Ice Shelf extracted from the Scientific Committee on Antarctic Research (SCAR) Met-READER project (<https://legacy.bas.ac.uk/met/READER/>). Monthly sea ice concentrations in the Wordie Bay area are extracted from the Bootstrap Sea Ice Concentrations dataset<sup>68</sup> derived from Nimbus-7 and Defense Meteorological Satellite Program (DMSP) satellites. Subsequently, we calculate the annual mean November to March sea ice concentration in the region.

To track the progression of ocean temperatures in the Marguerite Bay, we used Conductivity Temperature and Depth (CTD)

measurements obtained from the Hadley Centre ([bodc.ac.uk](http://bodc.ac.uk)) spanning the years 1960 to 2019. Using the temperature profiles, we calculated the average temperature within the 150–500 m depth range (Supplementary Fig. S13). We then used a locally weighted scatterplot smoothing<sup>69</sup> to plot the temporal evolution of the warm water layer through time.

## Data availability

All produced datasets are accessible at <https://doi.org/10.60612/DATADK/AEOFGC>. Monthly averaged RACMO2.3p2 variable are available at <https://zenodo.org/records/7760491>. Air temperatures from Rothera Station are available via the Scientific Committee on Antarctic Research (SCAR) Met-READER project <https://legacy.bas.ac.uk/met/READER/>. Additionally, mean monthly ERA5 data on 2-m air temperature can be downloaded via <https://cds.climate.copernicus.eu/datasets/reanalysis-eras-single-levels-monthly-means?tab=overview>. The historical aerial photos can be accessed via <https://www.pgc.umn.edu/data/aerial/>. MEaSUREs and ASaID grounding lines are available via <https://nsidc.org/data/nsidc-0498/versions/2> and <https://www.usap-dc.org/view/dataset/609489>, respectively. Sea ice concentration data is available at <https://nsidc.org/data/nsidc-0079/versions/4>. CTD data is available via Hadley Centre <https://www.bodc.ac.uk/>. Velocities from ITS\_LIVE is available via <https://nsidc.org/data/nsidc-0776/versions/1>. Landsat was provided free of charge by the U.S. Geological Survey Earth Resources Observation Science Center <https://earthexplorer.usgs.gov/>. ERS data can be downloaded via <https://earth.esa.int/eogateway>.

## References

- Fürst, J. J. et al. The safety band of Antarctic ice shelves. *Nat. Clim. Change* **6**, 479–482 (2016).
- Sun, S. et al. Antarctic ice sheet response to sudden and sustained ice-shelf collapse (ABUMIP). *J. Glaciol.* **66**, 891–904 (2020).
- North, R. & Barrows, T. T. High-resolution elevation models of Larsen B glaciers extracted from 1960s imagery. *Sci. Rep.* **14**, 14536 (2024).
- Mouginot, J., Rignot, E. & Scheuchl, B. Sustained increase in ice discharge from the Amundsen Sea Embayment, West Antarctica, from 1973 to 2013. *Geophys. Res. Lett.* **41**, 1576–1584 (2014).
- Rignot, E., Mouginot, J., Morlighem, M., Seroussi, H. & Scheuchl, B. Widespread, rapid grounding line retreat of Pine Island, Thwaites, Smith, and Kohler glaciers, West Antarctica, from 1992 to 2011. *Geophys. Res. Lett.* **41**, 3502–3509 (2014).
- Rignot, E. et al. Accelerated ice discharge from the Antarctic Peninsula following the collapse of Larsen B ice shelf. *Geophys. Res. Lett.* **31**, L18401 (2004).
- Cook, A. J. & Vaughan, D. G. Overview of areal changes of the ice shelves on the Antarctic Peninsula over the past 50 years. *Cryosphere* **4**, 77–98 (2010).
- Glasser, N. F. & Scambos, T. A. A structural glaciological analysis of the 2002 Larsen B ice-shelf collapse. *J. Glaciol.* **54**, 3–16 (2008).
- Wille, J. D. et al. Intense atmospheric rivers can weaken ice shelf stability at the Antarctic Peninsula. *Commun. Earth Environ.* **3**, 1–14 (2022).
- Lai, C.-Y. et al. Vulnerability of Antarctica's ice shelves to meltwater-driven fracture. *Nature* **584**, 574–578 (2020).
- Scambos, T. et al. Ice shelf disintegration by plate bending and hydro-fracture: Satellite observations and model results of the 2008 Wilkins ice shelf break-ups. *Earth Planet. Sci. Lett.* **280**, 51–60 (2009).
- Rignot, E. et al. Widespread seawater intrusions beneath the grounded ice of Thwaites Glacier, West Antarctica. *Proc. Natl Acad. Sci.* **121**, e2404766121 (2024).
- Pritchard, H. D. et al. Antarctic ice-sheet loss driven by basal melting of ice shelves. *Nature* **484**, 502–505 (2012).
- Larour, E., Rignot, E., Poinelli, M. & Scheuchl, B. Physical processes controlling the rifting of Larsen C Ice Shelf, Antarctica, prior to the calving of iceberg A68. *Proc. Natl Acad. Sci.* **118**, e2105080118 (2021).
- Massom, R. A. et al. Antarctic ice shelf disintegration triggered by sea ice loss and ocean swell. *Nature* **558**, 383–389 (2018).
- Lhermitte, S. et al. Damage accelerates ice shelf instability and mass loss in Amundsen Sea Embayment. *Proc. Natl Acad. Sci.* **117**, 24735–24741 (2020).
- Miles, B. W. J. et al. Intermittent structural weakening and acceleration of the Thwaites Glacier Tongue between 2000 and 2018. *J. Glaciol.* **66**, 485–495 (2020).
- Arthur, J. F. et al. The triggers of the disaggregation of Voyeykov Ice Shelf (2007), Wilkes Land, East Antarctica, and its subsequent evolution. *J. Glaciol.* **67**, 933–951 (2021).
- Doake, C. S. M. & Vaughan, D. G. Rapid disintegration of the Wordie Ice Shelf in response to atmospheric warming. *Nature* **350**, 328–330 (1991).
- Benn, D. I. et al. Rapid fragmentation of Thwaites Eastern Ice Shelf. *Cryosphere* **16**, 2545–2564 (2022).
- Walker, C. C. et al. Multi-decadal collapse of East Antarctica's Conger–Glenzer Ice Shelf. *Nat. Geosci.* **17**, 1240–1248 (2024).
- van de Wal, R. S. W. et al. A High-End Estimate of Sea Level Rise for Practitioners. *Earths Fut.* **10**, e2022EF002751 (2022).
- Bamber, J. L., Oppenheimer, M., Kopp, R. E., Aspinall, W. P. & Cooke, R. M. Ice sheet contributions to future sea-level rise from structured expert judgment. *Proc. Natl Acad. Sci.* **116**, 11195–11200 (2019).
- Byrd, R. E. & Saunders, H. E. The Flight to Marie Byrd Land: With a Description of the Map. *Geographical Rev.* **23**, 177 (1933).
- Christensen, L. *Min Siste Ekspedisjon Til Antarktis 1936-1937* (Oslo, 1938).
- Harris, U., Brolsma, H. & Smith, D. T. The collection of aerial photographs held by the Australian Antarctic Data Centre. [https://data.aad.gov.au/metadata/aerial\\_photo\\_gis](https://data.aad.gov.au/metadata/aerial_photo_gis), Accessed: 2025-04-22 (2000).
- Earth Resources Observation And Science (EROS) Center. Antarctic Single Frames. U.S. Geological Survey <https://doi.org/10.5066/F7MW2FDP> (2017).
- Dømggaard, M. et al. Early aerial expedition photos reveal 85 years of glacier growth and stability in East Antarctica. *Nat. Commun.* **15**, 4466 (2024).
- Child, S. F., Stearns, L. A., Girod, L. & Brecher, H. H. Structure-From-Motion Photogrammetry of Antarctic Historical Aerial Photographs in Conjunction with Ground Control Derived from Satellite Data. *Remote Sens.* **13**, 21 (2020).
- Wendt, J. et al. Recent ice-surface-elevation changes of Fleming Glacier in response to the removal of the Wordie Ice Shelf, Antarctic Peninsula. *Ann. Glaciol.* **51**, 97–102 (2010).
- Walker, C. C. & Gardner, A. S. Rapid drawdown of Antarctica's Wordie Ice Shelf glaciers in response to ENSO/Southern Annular Mode-driven warming in the Southern Ocean. *Earth Planet. Sci. Lett.* **476**, 100–110 (2017).
- Rignot, E. et al. Recent ice loss from the Fleming and other glaciers, Wordie Bay, West Antarctic Peninsula. *Geophys. Res. Lett.* **32**, L07502 (2005).
- Friedl, P., Seehaus, T. C., Wendt, A., Braun, M. H. & Höppner, K. Recent dynamic changes on Fleming Glacier after the disintegration of Wordie Ice Shelf, Antarctic Peninsula. *Cryosphere* **12**, 1347–1365 (2018).
- Scambos, T. A., Hulbe, C., Fahnestock, M. & Bohlander, J. The link between climate warming and break-up of ice shelves in the Antarctic Peninsula. *J. Glaciol.* **46**, 516–530 (2000).
- Morris, E. M. & Vaughan, D. G. Spatial and Temporal Variation of Surface Temperature on the Antarctic Peninsula And The Limit of

- Viability of Ice Shelves. In: *Antarctic Research Series* (eds. Domack, E. et al.) 61–68 (American Geophysical Union, Washington, D. C., 2003). <https://doi.org/10.1029/AR079p0061>.
36. Leeson, A. A., Forster, E., Rice, A., Gourmelen, N. & van Wessem, J. M. Evolution of Supraglacial Lakes on the Larsen B Ice Shelf in the Decades Before it Collapsed. *Geophys. Res. Lett.* **47**, e2019GL085591 (2020).
  37. Schneider, D. P. & Fogt, R. L. Artifacts in Century-Length Atmospheric and Coupled Reanalyses Over Antarctica Due To Historical Data Availability. *Geophys. Res. Lett.* **45**, 964–973 (2018).
  38. Miles, B. W. J. & Bingham, R. G. Progressive unanchoring of Antarctic ice shelves since 1973. *Nature* **626**, 785–791 (2024).
  39. Rignot, E., Jacobs, S., Mouginot, J. & Scheuchl, B. Ice-Shelf Melting Around Antarctica. *Science* **341**, 266–270 (2013).
  40. Rignot, E. & Jacobs, S. S. Rapid Bottom Melting Widespread near Antarctic Ice Sheet Grounding Lines. *Science* **296**, 2020–2023 (2002).
  41. Padman, L. et al. Oceanic controls on the mass balance of Wilkins Ice Shelf, Antarctica. *J. Geophys. Res. Oceans* **117**, C01010 (2012).
  42. Sun, Y., Riel, B. & Minchew, B. Disintegration and Buttrressing Effect of the Landfast Sea Ice in the Larsen B Embayment, Antarctic Peninsula. *Geophys. Res. Lett.* **50**, e2023GL104066 (2023).
  43. Scambos, T. A., Bohlander, J. A., Shuman, C. A. & Skvarca, P. Glacier acceleration and thinning after ice shelf collapse in the Larsen B embayment, Antarctica. *Geophys. Res. Lett.* **31**, L18402 (2004).
  44. Rignot, E. et al. Four decades of Antarctic Ice Sheet mass balance from 1979–2017. *Proc. Natl Acad. Sci. USA* **116**, 1095–1103 (2019).
  45. Cook, A. J., Fox, A. J., Vaughan, D. G. & Ferrigno, J. G. Retreating Glacier Fronts on the Antarctic Peninsula over the Past Half-Century. *Science* **308**, 541–544 (2005).
  46. Cook, A. J. et al. Ocean forcing of glacier retreat in the western Antarctic Peninsula. *Science* **353**, 283–286 (2016).
  47. Wood, M. et al. Ocean forcing drives glacier retreat in Greenland. *Sci. Adv.* **7**, eaba7282 (2021).
  48. Agisoft Metashape. *Agisoft Metashape User Manual - Professional Edition*, Version 2.1. (Agisoft Metashape, 2024).
  49. Howat, I. M., Porter, C., Smith, B. E., Noh, M.-J. & Morin, P. The Reference Elevation Model of Antarctica. *Cryosphere* **13**, 665–674 (2019).
  50. Nuth, C. & Kääb, A. Co-registration and bias corrections of satellite elevation data sets for quantifying glacier thickness change. *Cryosphere* **5**, 271–290 (2011).
  51. Hugonnet, R. et al. Uncertainty Analysis of Digital Elevation Models by Spatial Inference From Stable Terrain. *IEEE J. Sel. Top. Appl. Earth Observ. Remote Sens.* **15**, 6456–6472 (2022).
  52. Korona, J., Berthier, E., Bernard, M., Rémy, F. & Thouvenot, E. SPIRIT. SPOT 5 stereoscopic survey of Polar Ice: Reference Images and Topographies during the fourth International Polar Year (2007–2009). *ISPRS J. Photogramm. Remote Sens.* **64**, 204–212 (2009).
  53. Bernat, M. et al. Geodetic mass balance of Mýrdalsjökull ice cap, 1999–2021. *J.ök.* **73**, 35–53 (2023).
  54. Mouginot, J., Björk, A. A., Millan, R., Scheuchl, B. & Rignot, E. Insights on the Surge Behavior of Storstrømmen and L. Bistrup Bræ, Northeast Greenland, Over the Last Century. *Geophys. Res. Lett.* **45**, 11,197–11,205 (2018).
  55. Rignot, E. & University Of California Irvine. MEaSURES Antarctic Grounding Line from Differential Satellite Radar Interferometry, Version 2. NASA National Snow and Ice Data Center Distributed Active Archive Center, <https://doi.org/10.5067/IKBWW4RYHF1Q> (2016).
  56. Bindshadler, R. & Choi, H. High-resolution Image-derived Grounding and Hydrostatic Lines for the Antarctic Ice Sheet. U.S. Antarctic Program Data Center (USAP-DC), via National Snow and Ice Data Center (NSIDC), <https://doi.org/10.7265/N56T0JK2> (2011).
  57. Bindshadler, R. et al. Getting around Antarctica: new high-resolution mappings of the grounded and freely-floating boundaries of the Antarctic ice sheet created for the International Polar Year. *Cryosphere* **5**, 569–588 (2011).
  58. Rignot, E. Tidal motion, ice velocity and melt rate of Petermann Gletscher, Greenland, measured from radar interferometry. *J. Glaciol.* **42**, 476–485 (1996).
  59. Joughin, I., Smith, B. E. & Holland, D. M. Sensitivity of 21st century sea level to ocean-induced thinning of Pine Island Glacier, Antarctica. *Geophys. Res. Lett.* **37**, 2010GL044819 (2010).
  60. Friedl, P., Weiser, F., Fluhrer, A. & Braun, M. H. Remote sensing of glacier and ice sheet grounding lines: A review. *Earth Sci. Rev.* **201**, 102948 (2020).
  61. Mouginot, J., Scheuchl, B. & Rignot, E. Mapping of Ice Motion in Antarctica Using Synthetic-Aperture Radar Data. *Remote Sens.* **4**, 2753–2767 (2012).
  62. Mouginot, J., Rignot, E., Scheuchl, B. & Millan, R. Comprehensive Annual Ice Sheet Velocity Mapping Using Landsat-8, Sentinel-1, and RADARSAT-2 Data. *Remote Sens.* **9**, 364 (2017).
  63. Millan, R. et al. Mapping Surface Flow Velocity of Glaciers at Regional Scale Using a Multiple Sensors Approach. *Remote Sens.* **11**, 2498 (2019).
  64. Gardner, A., Fahnestock, M. & Scambos, T. Measures its\_live Regional Glacier and Ice Sheet Surface Velocities, Version 1. NASA National Snow and Ice Data Center DAAC <https://doi.org/10.5067/6II6VW8LLWJ7> (2022).
  65. Matsuoka, K. et al. Antarctic ice rises and rumples: Their properties and significance for ice-sheet dynamics and evolution. *Earth-Sci. Rev.* **150**, 724–745 (2015).
  66. van Wessem, J. M. et al. Modelling the climate and surface mass balance of polar ice sheets using RACMO2 – Part 2: Antarctica (1979–2016). *Cryosphere* **12**, 1479–1498 (2018).
  67. Hersbach, H. et al. ERA5 monthly averaged data on single levels from 1940 to present. ECMWF <https://doi.org/10.24381/CDS.F17050D7> (2023).
  68. Comiso, J. C. & Gersten, R. A. Bootstrap Sea Ice Concentrations from Nimbus-7 SMMR and DMSP SSM/I-SSMIS, Version 4. NASA National Snow and Ice Data Center Distributed Active Archive Center <https://doi.org/10.5067/X5LG68MH0130> (2023).
  69. Derkacheva, A., Mouginot, J., Millan, R., Maier, N. & Gillet-Chaulet, F. Data Reduction Using Statistical and Regression Approaches for Ice Velocity Derived by Landsat-8, Sentinel-1 and Sentinel-2. *Remote Sens.* **12**, 1935 (2020).
  70. Matsuoka, K. et al. Quantarctica, an integrated mapping environment for Antarctica, the Southern Ocean, and sub-Antarctic islands. *Environ. Model. Softw.* **140**, 105015 (2021).

## Acknowledgements

This work was funded by the Villum Foundation (Villum Young Investigator grant no. 29456), received by AAB. R.M acknowledges support from the European Research Council (ERC) under the Horizon Framework research and innovation program of the European Union (grant no. 101164392; “IceDaM” project).

## Author contributions

M.D., R.M., and A.A.B., designed the study. M.D. led the data analysis and wrote the main manuscript, with inputs from R.M., and A.A.B. All authors (M.D., R.M., J.K.A., B.S., E.S., M.I., M.B., and A.A.B.) contributed to writing the manuscript and interpreting the results.

## Competing interests

The authors declare no competing interests.



## Additional information

**Supplementary information** The online version contains supplementary material available at <https://doi.org/10.1038/s41467-025-59293-1>.

**Correspondence** and requests for materials should be addressed to Mads Dømggaard.

**Peer review information** *Nature Communications* thanks Jennifer Arthur, Ted Scambos and the other, anonymous, reviewer(s) for their contribution to the peer review of this work. A peer review file is available.

**Reprints and permissions information** is available at <http://www.nature.com/reprints>

**Publisher's note** Springer Nature remains neutral with regard to jurisdictional claims in published maps and institutional affiliations.

**Open Access** This article is licensed under a Creative Commons Attribution-NonCommercial-NoDerivatives 4.0 International License, which permits any non-commercial use, sharing, distribution and reproduction in any medium or format, as long as you give appropriate credit to the original author(s) and the source, provide a link to the Creative Commons licence, and indicate if you modified the licensed material. You do not have permission under this licence to share adapted material derived from this article or parts of it. The images or other third party material in this article are included in the article's Creative Commons licence, unless indicated otherwise in a credit line to the material. If material is not included in the article's Creative Commons licence and your intended use is not permitted by statutory regulation or exceeds the permitted use, you will need to obtain permission directly from the copyright holder. To view a copy of this licence, visit <http://creativecommons.org/licenses/by-nc-nd/4.0/>.

© The Author(s) 2025